

# Effects of surface coating on the shortwave and longwave radiative effects of dust aerosol in comparison with external mixing: A theoretical study

Zhibo Zhang<sup>1,2,\*</sup>, Qianqian Song<sup>3</sup>, Jianyu Zheng<sup>2</sup>, Hongbin Yu<sup>4</sup>

1. Physics Department, University of Maryland Baltimore County (UMBC), Baltimore, Maryland, U.S.
2. Goddard Earth Sciences Technology and Research, UMBC, Baltimore, Maryland, U.S.
3. Atmospheric and Oceanic Sciences Program, Princeton, New Jersey, US
4. Climate and Radiation Laboratory, NASA Goddard Space Flight Center, Greenbelt, Maryland, US.

\* Corresponding author: [zhibo.zhang@umbc.edu](mailto:zhibo.zhang@umbc.edu)

## Highlights

- Local pollutants can coat on transported dust particles to form a surface coating layer
- In comparison with external mixing, coated dust particles have a weaker shortwave cooling effect and a stronger longwave warming effect at the top of atmosphere and surface
- Surface coating enhances the shortwave absorption of dust particles through the lensing effect

## Abstract

Dust particles can be coated with a surface layer of pollutants such as sulfate and nitrate after mixing with local pollution during long-range transport. Previous studies investigated the effects of surface coating on scattering properties and direct radiative effects (DRE) of dust in the solar shortwave (SW) spectral region. In this research, we carried out a theoretical study of the surface coating effects in both solar SW and the terrestrial longwave (LW) and compared the results with external mixing. Three dust coating schemes were developed to study a hypothetical sulfate-dust coating case, in which the thickness of the coating sulfate layer is proportional to the size, surface area, and mass of the dust core, respectively. We found that at the 0.55  $\mu\text{m}$  the aerosol optical thickness (AOD) of the externally mixed dust-sulfate increases more efficiently with the increasing sulfate mass than the coated dust cases, whereas the opposite is true at the 10  $\mu\text{m}$ . This is because at 0.55  $\mu\text{m}$  the difference in the total geometrical cross section is the dominant factor for the AOD difference, while at the 10  $\mu\text{m}$  the dominant factor is the difference in extinction cross section. The differences in dust DRE at the top of atmosphere and surface between the external mixing and coated dust cases can be largely explained by the differences in AOD. Dust absorption in the SW is found to be significantly enhanced by the surface coating of non-absorptive sulfate

Formatted: Outline numbered + Level: 1 + Numbering  
Style: 1, 2, 3, ... + Start at: 1 + Alignment: Left + Aligned  
at: 0.25" + Indent at: 0.5"

Formatted: Outline numbered + Level: 1 + Numbering  
Style: Bullet + Aligned at: 0.25" + Indent at: 0.5"

35 due to the so-called “lensing effect”. When SW and LW DREs are combined, the volume- and  
36 area-proportional coating schemes have a significantly weaker cooling effect than externally  
37 mixed dust-sulfate. This research provides the theoretical understanding of how surface coating  
38 affects the SW, LW and total dust DREs.

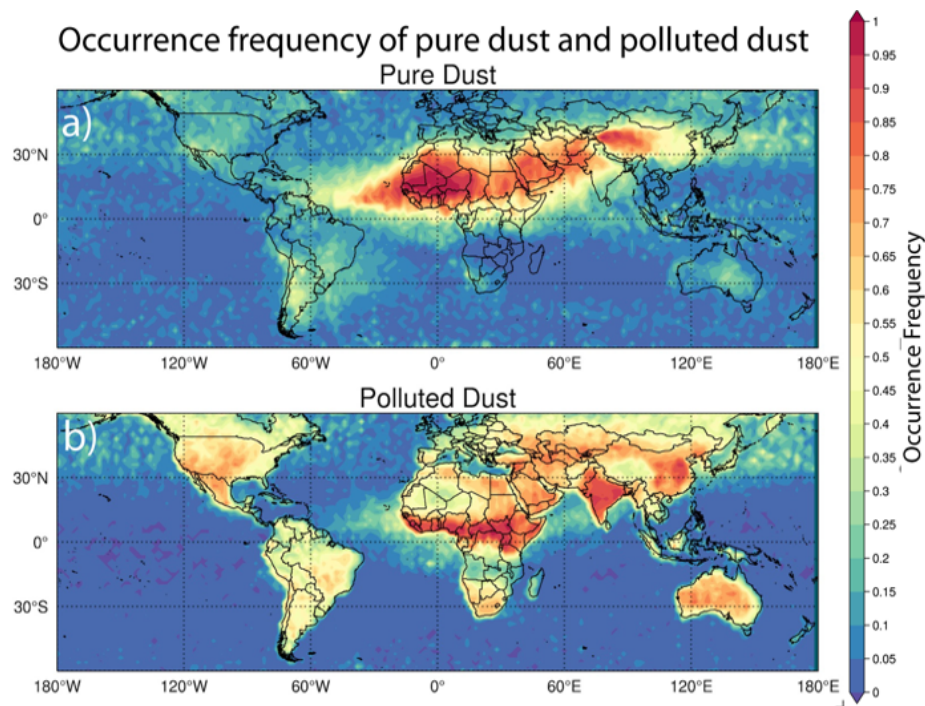
## 1. Introduction

Mineral dust (referred to as dust for short) is one of the most abundant types of atmospheric aerosols [1], [2]. Different from most other types of aerosols that have significant radiative effects only in the solar shortwave (SW) region, dust interacts with both SW and thermal infrared (IR) longwave (LW) radiation and thereby influences the Earth's radiative energy budget. The direct radiative effect (DRE) of dust is generally negative (i.e., cooling) at SW (i.e.,  $DRE_{SW} < 0$ ) and positive (warming) at LW (i.e.,  $DRE_{LW} > 0$ ). [3–6]. In addition to the DRE, dust also influences the life cycle and properties of clouds by altering the thermal structure of the atmosphere through dust-radiation interactions [7,8] and by acting as cloud condensation nuclei (CCN) and ice nuclei (IN), which is known as the aerosol-cloud interactions (ACI) [9,10].

Once aloft, dust particles are often carried by winds for long-range transport at an intercontinental or even hemispherical scale, such as the trans-Atlantic transport of African dust, trans-pacific transport of Asia dust, and transport of dust plumes from the Arabian Peninsula over the Arabian Sea and the Indian Ocean [11–13]. During the transport, the dust particles can become mixed with local pollutants such as ammonium sulfate, ammonium nitrate, hydrochloric acid, and biomass burning particles, not only externally but also internally through heterogeneous reactions and coagulation [14–19]. Figure 1 shows the occurrence frequency of pure dust and dust-pollutant mixture (i.e., “polluted dust”) based on the observations from the space-borne Cloud-Aerosol Lidar with Orthogonal Polarization (CALIOP) [20]. Note that in this study “pure dust” refers to those dust particles without being either internally or externally mixed with other aerosols. As expected, pure dust (Figure 1a) is the dominant type of aerosols in the so-called “dust belt”, which expands across North Africa, the Middle East and to inland Asia. The mixtures of dust with local pollutants (Figure 1b), categorized as the “polluted dust” in the CALIOP product, is frequently

Formatted: Outline numbered + Level: 1 + Numbering  
Style: 1, 2, 3, ... + Start at: 1 + Alignment: Right + Aligned  
at: 0.25" + Indent at: 0.5"

63 observed over India, east China, and central Africa, which happen to be the downwind of dust  
64 sources and at the same time highly polluted regions.



65  
66 **Figure 1.** Occurrence frequency of “pure dust” and “polluted dust” based on 5 km resolution  
67 CALIOP level-2 aerosol layer product (CAL\_LID\_L2\_05kmALay). The occurrence frequency is  
68 defined as the ratio of number of the cloud-free pure dust (or polluted dust) profiles with respect  
69 to the total cloud-free aerosol profiles number.  
70

71 Dust particles can interact with pollutants in various ways, leading to changes of dust composition  
72 and hygroscopicity which in turn influence how dust interacts with water. Laboratory studies have  
73 demonstrated the dust uptake of a variety of trace gasses through gas-solid heterogeneous  
74 reactions, including  $\text{NO}_x$ ,  $\text{NO}_y$  (e.g.,  $\text{HNO}_3$  and  $\text{NO}_3$ ) and  $\text{SO}_2$  [14,21–24]. Dust-pollution-water  
75 interactions have profound effects on dust microphysical properties, including size, morphology.

76 Using the transmission electron microscopy (TEM) technique, [Li and Shao](#) [17] found that  
77 approximately 90% of the dust particles collected during the hazy days of Beijing are covered by  
78 visible nitrate coatings. The coating of hygroscopic material promotes water absorption, often  
79 creating a thin aqueous layer on the surface of dust. The coating layer makes dust particles larger,  
80 smoother, and more spherical, in comparison with uncoated pure dust. The changes of  
81 microphysical properties because of the dust-pollution-water interactions could have significant  
82 impacts on dust scattering properties and important implications for climate studies and dust  
83 remote sensing. First, the changes of dust size, morphology, and composition can influence the  
84 local and even global radiative energy balance through dust radiative effects [25]. Second, the  
85 mixing state can also influence dust's potential as CCN and IN. In particular, the coating of dust  
86 with hydrophilic aerosols such as ammonium nitrate can make dust a less effective IN and a better  
87 CCN [10,26]. Furthermore, the differences in the scattering properties, such as the lidar  
88 depolarization ratio (LDR) of different dust mixtures can pose great challenges, but at the same  
89 time provide valuable opportunities for the remote sensing observations of dust [19,27].

90  
91 This study concerns the impacts of internal mixing of dust with other aerosols, namely surface  
92 coating of dust by pollutants (e.g., sulfate and ammonium nitrate), on the scattering properties  
93 and DRE of dust. In particular, we are interested in the effects of surface coating on both SW and  
94 LW dust DREs, and how the DREs of coated dust are compared to those of externally mixed dust.  
95 Most previous studies focused on the effects of dust surface coating in the SW. For example,  
96 [Bauer et al.](#) [28] simulated the scattering properties of coated dust as core-mantle spherical  
97 particles using a Mie-type code. They found that in comparison with pure (i.e., uncoated) dust  
98 particles with the same size, the coated dust tends to have larger SW single scattering albedo  
99 (SSA) and smaller asymmetry factor in the SW region from 300 nm to 2000 nm. After  
100 implementing the coated dust in a global climate model, [Bauer et al.](#) [28] showed that the coating

101 of sulfate and nitrate on dust surfaces leads to a strong reduction of the strength of combined  
102 anthropogenic SW DRE of dust, nitrate, and sulfate, from  $-0.3 \text{ W m}^{-2}$  when coating is turned off in  
103 the model to  $-0.1 \text{ W m}^{-2}$  when it is allowed. More recently, [Tian et al. \[24\]](#) studied the AERONET  
104 (AErosol RObotic NETwork) retrievals of dust-pollution mixture in East Asia. They found that dust-  
105 pollution mixtures exhibit significantly enhanced absorbing ability than the corresponding unmixed  
106 dust and anthropogenic aerosols. In contrast to these studies focusing on the SW DRE, no  
107 previous studies have investigated the impacts of mixing state on the LW DRE of dust. Recently,  
108 there are an increasing number of studies suggesting that the LW DRE of dust is comparable in  
109 magnitude to the SW DRE of dust [4,29,30]. In the light of these studies, an understanding of  
110 how the mixing state affects the LW dust DRE becomes an important and necessary step in  
111 understanding the net DRE and thereby climate effects of dust. In this paper, we aim to lay out a  
112 theoretical foundation in this paper to understand the contrasting impacts of external and internal  
113 mixing of dust with pollution aerosols on SW, LW and therefore net DRE of dust.

114

## 115 2. Schemes for dust mixing with pollution aerosols

116 In previous studies of dust DRE, polluted dust is often treated as an external mixture of dust and  
117 pollution aerosols [31,32]. For example, based on the assumption of external mixing [Song et al.](#)  
118 ([32]) utilized the fact that pure dust aerosols are nonspherical and therefore have a significantly  
119 larger lidar depolarization ratio than pollution aerosols (e.g., sulfate and nitrate) to separate the  
120 dust extinction from the total extinction profile retrieved from the CALIOP. The resulting dust  
121 extinction profiles were later used in [Song et al. \[30\]](#) to estimate the DRE of dust aerosols.  
122 However, since a significant fraction of the polluted dust is likely to be an internal mixture, namely  
123 dust particles coated with pollution aerosols. In order to understand the impacts of surface coating  
124 on dust DRE in SW and LW we first develop a simple theoretical model to simulate the coating of

Formatted: Outline numbered + Level: 1 + Numbering  
Style: 1, 2, 3, ... + Start at: 1 + Alignment: Right + Aligned  
at: 0.25" + Indent at: 0.5"

125 pollution aerosols on the surface of dust and then use it to guide the computations of dust  
126 scattering properties and DRE.

127

128 Following previous studies, we use the concentric spherical core-shell model to simulate the  
129 surface coating of pollution on dust cores [28]. Although this is certainly a simplified and idealized  
130 model, we believe it is sufficient to provide valuable insights into the effects of surface coating on  
131 dust DRE. On the other hand, we note the caveat that dust shape can have significant impacts  
132 on dust DRE and plan to use more complex dust shape in figure studies. As explained in the next  
133 section, the concentric spherical core-shell model also helps simplify the computation of the  
134 scattering properties of coated dust particles. As shown in Fig. 2 (yellow curves), the particle size  
135 distribution (PSD) of dust cores is assumed to follow the global mean atmospheric dust PSD as  
136 reported in Kok et al., [4], which is derived from the experimental constrained globally averaged  
137 dust PSD at emission and modeling constrained globally averaged size-resolved dust lifetime  
138 (see Kok et al., [4] for more details). The aerosol optical depth (AOD) of pure dust cores is  
139 assumed to be 0.2 at 550 nm. The pollution aerosol is assumed to be sulfate. For comparison  
140 purposes, we first set up an external mixing experiment in which the sulfate aerosols (with size  
141  $D_s$ ) are assumed to have a log-normal PSD with an effective size of 0.33  $\mu\text{m}$  (blue curves in Fig.  
142 2).

143

144 In case of external mixing, the scattering and radiative properties of the mixture are computed  
145 based on the simple averages of the two components. For example, the total AOD of the external  
146 mixture ( $\tau$ ) is the sum of the dust ( $\tau_d$ ) and sulfate ( $\tau_s$ ) AOD, i.e.,  $\tau = \tau_d + \tau_s$ . The single scattering  
147 albedo of the external mixture is given by  $\omega = (\omega_d \tau_d + \omega_s \tau_s) / \tau$ . In the experiments, a number  
148 of progressively increasing masses of sulfate aerosols are tested to study the corresponding  
149 impacts on the scattering properties of the mixture and the corresponding DREs.

150

**Deleted:** Dust cores are assumed to be spherical for simplicity. As shown in previous studies, although dust particle shape is important for dust remote sensing, it has only limited impacts on dust DREs [5,30]. As explained in the next selection

156 To compare with the external mixing results, we develop three different internal mixing schemes  
 157 in which sulfate is coated on a dust core to form a concentric spherical core-shell particle (referred  
 158 to as coated dust hereafter). To make the results comparable to the external mixing counterpart,  
 159 we keep the following quantities conserved in the mixing schemes: First, both total number and  
 160 volume of dust cores are conserved; Second, the total volume and therefore mass of sulfate  
 161 aerosols are conserved. The three different coating schemes, as summarized in Table 1,  
 162 represent our attempts to capture the potential variability of coating as a result of different physical  
 163 processes. From a different perspective, because our understanding and measurements of dust  
 164 coating are still limited, the three different mixing schemes can be considered as an estimation of  
 165 the uncertainty due to our limited knowledge. In scheme 1, the sulfate shell volume on each dust  
 166 core is assumed to be proportional to the size of the dust core (referred to as “size-proportional  
 167 coating”), i.e.,  $V_{shell}(D_{core}) = C_1 \cdot D_{core}$ ; In scheme 2, the sulfate shell volume on each dust core  
 168 is proportional to the surface area of the dust core (referred to as “area-proportional coating”), i.e.,  
 169  $V_{shell}(D_{core}) = C_2 \cdot D_{core}^2$ ; In scheme 3, the sulfate shell volume is proportional to the surface  
 170 volume of dust core (referred to as “volume-proportional coating”),  $V_{shell}(D_{core}) = C_3 \cdot D_{core}^3$ . The  
 171 three constant parameters,  $C_1$ ,  $C_2$  and  $C_3$  (referred to as “coating constant”) are diagnosed based  
 172 on the sulfate volume conservation equation

$$\int_0^{\infty} V_{shell}(D_{core}) \cdot n(D_{core}) d \ln D_{core} = V_{sulfate} \quad (1)$$

174 On the left hand side of the above questions,  $V_{shell}(D_{core})$  is the volume of the sulfate shell  
 175 coated on the dust core with the size of  $D_{core}$ ,  $n(D_{core}) = dN/d \ln D_{core}$  is the size distribution of  
 176 the dust core. On the right hand side,  $V_{sulfate} = \int_0^{\infty} V_{shell}(D_s) \cdot n(D_s) d \ln D_s$  is the total volume of  
 177 sulfate aerosol integrated over its PSD  $n(D_s)$ , which is assumed to be conserved for a given

Formatted Table



178 sulfate AOD. After the coating constants are diagnosed, the size of a coated dust ( $D_{coated}$ ) with a  
179 given dust core  $D_{core}$  and therefore the whole PSD of the coated dust ( $n(D_{coated})$ ) can be  
180 specified for each coating scheme. Different from the external mixing whose scattering properties  
181 are simple averages of dust and sulfate aerosols, the scattering properties of the coated dust  
182 need to be computed using a specialized Mie-type scattering model that will be introduced in  
183 Section 3.

185 **Table 1:** Three different dust coating schemes.

<b>Scheme 1</b>	Coating proportional to dust size	$V_{shell}(D_{core}) = C_1 \cdot D_{core}$
<b>Scheme 2</b>	Coating proportional to dust surface area	$V_{shell}(D_{core}) = C_2 \cdot D_{core}^2$
<b>Scheme 3</b>	Coating proportional to dust volume	$V_{shell}(D_{core}) = C_3 \cdot D_{core}^3$

Formatted Table

187  
188 The three coating schemes are further explained using the examples in Figure 2. In the examples,  
189 the AOD of sulfate aerosol (blue dotted line) is assumed to be 0.2 at 0.55  $\mu\text{m}$ , same as that of  
190 dust (orange dashed line). The PSDs of coated dust based on three different coating schemes  
191 are represented by the black lines. In the size-proportional coating scheme (first row of Figure 2),  
192 because the volume of the coated sulfate shell is proportional to the size of the dust core, the  
193 relative size growth, measured by  $(1 + \Delta_{shell}/D_{core})^3$  with  $\Delta_{shell}$  corresponding to the thickness  
194 of sulfate shell, is inversely proportional to  $D_{core}^2$ , i.e.,  $(1 + \Delta_{shell}/D_{core})^3 \sim 1/D_{core}^2$ . In other

195 words, the smaller dust cores grow much faster than the larger ones. As a result, the PSD of the  
 196 coated dust is significantly narrower than that of the dust core and shifts slightly to the larger sizes.  
 197 In the volume-proportional coating mixing scheme (third row of Figure 2), because the volume of  
 198 the coated sulfate shell is proportional to the volume of the dust core, the relative size growth  
 199  $\Delta_{shell}/D_{core}$  is a constant. As a result, the PSD of the coated dust is simply shifted to the larger  
 200 size. The PSD of the coated dust based on the area-proportional mixing scheme (second row) is  
 201 somewhat in between those based on the size- and volume-proportional schemes, demonstrating  
 202 both narrowing and shifting to the larger sizes in comparison with the dust core PSD.

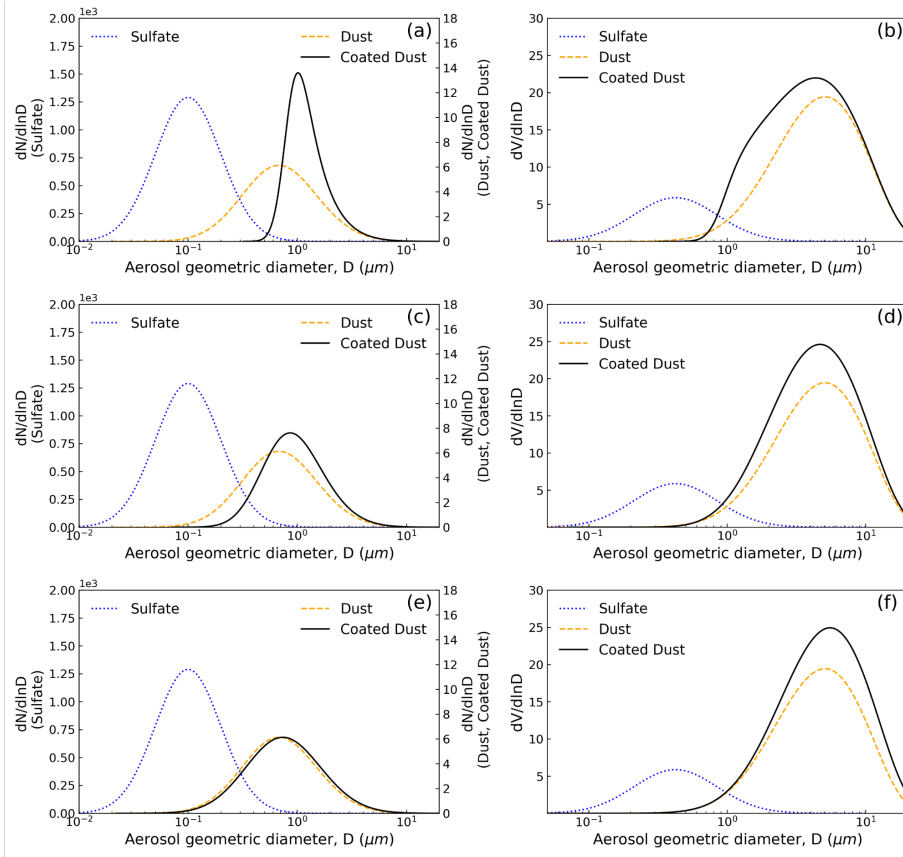


**Figure 2:** The PSD of sulfate , dust, and coated dust based on the three different coating schemes as summarized in Table 1. Each row represents one scheme from scheme 1 to scheme 3. The left column is for the number size distribution ( $dN/d\ln D$ ) in the unit of  $cm^{-3}$  and right column for volume size distribution ( $dV/d\ln D$ ) in the unit of  $\mu m^3 cm^{-3}$ . The blue dotted line and orange dashed line represent the PSD for sulfate aerosols and dust aerosols in the case of externally mixing, respectively. The black curves represent the corresponding PSD of coated dust (i.e., core-shell mixture) in each coating scheme.

### 3. Impacts of mixing state on the scattering properties of dust in SW and LW

As explained above, the scattering properties of the external mixture can be readily derived from those of dust and sulfate components. For the example in Figure 2, the total AOD of the external mixture is simply 0.4 as the simple summation of dust and sulfate AOD. For references, the bulk extinction efficiency ( $\langle Q_e \rangle$ ) of pure dust and sulfate aerosols following the PSDs in Figure 2 are given in Table 2 for two wavelengths at 0.55  $\mu m$  and 10  $\mu m$  which represent the typical visible and thermal infrared spectral regions, respectively. An important point to note is that although significantly smaller the  $\langle Q_e \rangle$  of sulfate at 0.55  $\mu m$  is on the same order of magnitude as that of dust, but at 10  $\mu m$  it is an order of magnitude smaller.

**Table 2** Bulk extinction efficiency of dust and sulfate based on the PSDs in Figure 2 at 0.55  $\mu m$  and 10  $\mu m$ .

	0.55 $\mu m$	10.0 $\mu m$
Dust	$\langle Q_e \rangle = 2.45$ $\langle \omega \rangle = 0.95$ 1.52 – i 1.54 $\times 10^{-3}$ (DB2019 Mean)	$\langle Q_e \rangle = 1.16$ $\langle \omega \rangle = 0.40$ 1.70 – i 0.33 (DB2017 Mean)
Sulfate	$\langle Q_e \rangle = 0.87$ $\langle \omega \rangle = 1.0$	$\langle Q_e \rangle = 0.035$ $\langle \omega \rangle = 0.01$

Formatted: Outline numbered + Level: 1 + Numbering Style: 1, 2, 3, ... + Start at: 1 + Alignment: Right + Aligned at: 0.25" + Indent at: 0.5"

Formatted Table

	1.358 – $i$ 4.044 $\times 10^{-9}$ (70%RH) <a href="https://cds-espri.ipsl.upmc.fr/etherTypo/?id=991">https://cds- espri.ipsl.upmc.fr/etherTypo/?id=991</a>	1.392 – $i$ 0.1556 (70% RH) <a href="https://cds-espri.ipsl.upmc.fr/etherTypo/?id=991">https://cds- espri.ipsl.upmc.fr/etherTypo/?id=991</a>
--	--	---

In contrast to external mixing, the scattering properties of coated dust need to be computed using advanced scattering models. In this study, we use an open-source Mie-type code implemented in a Python package—PyMieScatt [33]—to compute the scattering properties, such as extinction efficiency ( $\langle Q_e \rangle$ ), single scattering albedo ( $\langle \omega \rangle$ ) and asymmetry factor ( $\langle g \rangle$ ), of coated dusts that are modeled as concentric spherical core-shell particles. To this end, we first compute the single scattering properties, e.g.,  $Q_e$ ,  $\omega$  and  $g$ , of individual coated dust particles with the corresponding sulfate  $V_{shell}$  that is dependent on the mixing scheme used and the size of the dust core ( $R_{core}$ ) (see the previous section for detail). Then, the single scattering properties are averaged over the PSD of coated dusts (e.g., solid black curves in Figure 2) to obtain the corresponding bulk scattering properties  $\langle Q_e \rangle$ ,  $\langle \omega \rangle$  and  $\langle g \rangle$ . The AOD of the coated dust is therefore  $\tau_{coated} = \langle Q_e \rangle \cdot G_{total}$  where  $G_{total}$  is the vertically integrated total cross section of coated dust  $G_{total} = \int_0^\infty A(D_{coated}) \cdot n(D_{coated}) d \ln D_{coated} \cdot \Delta z$ .

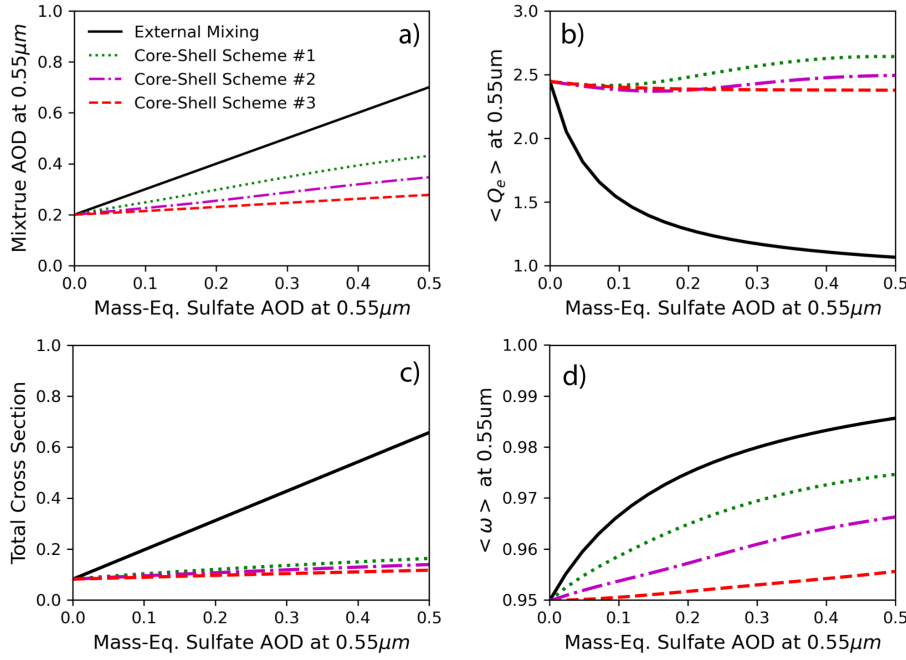
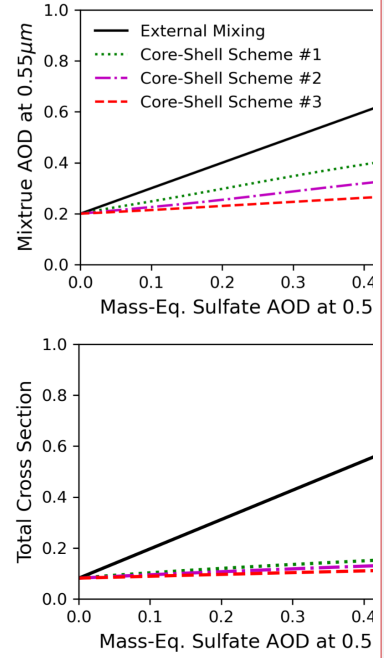


**Figure 3** Variation of a) AOD b)  $\langle Q_e \rangle$ , c)  $G_{total}$  d)  $\langle \omega \rangle$  as a function of mass-equivalent sulfate AOD at  $0.55\mu\text{m}$ .

Following these steps, we computed the bulk scattering properties for the coated dust based on the three coating schemes for a case with a fixed dust AOD  $\tau_d = 0.2$  at  $0.55\mu\text{m}$  and progressively increasing sulfate AOD from 0 to 0.5 at  $0.55\mu\text{m}$ . The results for the  $0.55\mu\text{m}$  wavelength are shown in Figure 3. As expected, the AOD of the external mixing (thick black line in Figure 3a) increases linearly with the sulfate AOD. Evidently, its magnitudes and increasing rate are significantly larger than those of all three coated dust cases. Because AOD is a product of extinction efficiency  $\langle Q_e \rangle$  and vertical integrated total cross section of particles, i.e.,  $AOD = \langle Q_e \rangle \cdot G_{total}$ , it is an important to understand which one,  $\langle Q_e \rangle$  or  $G_{total}$ , is the dominant factor that causes the large difference between external mixing and the coated dust cases. This is



Deleted:

253 investigated in Figure 3 b and c that decompose the AOD into  $\langle Q_e \rangle$  or  $G_{total}$ , respectively. As  
 254 expected, the  $\langle Q_e \rangle$  of the external mixture (thick black line) in Figure b reduces gradually from  
 255 the value of pure dust as more sulfate is added to mixture approaching eventually the  $\langle Q_e \rangle$  of  
 256 pure sulfate. Evidently, the  $\langle Q_e \rangle$  of the external mixture is consistently smaller than those of  
 257 coated dust. It implies that the larger AOD of the external mixture must be caused by the  
 258 difference in cross section  $G_{total}$ . This is indeed confirmed by Figure 3 c which shows that the  
 259  $G_{total}$  the external mixture is much larger and increases faster than those of coated dust when  
 260 more sulfate is added. Recall that in both external mixture and coated dust cases the total volume  
 261 of the sulfate is conserved. The total cross section area of the added sulfate aerosols is much  
 262 larger in the case of external mixing in the form of numerous tiny particles, compared to the coated  
 263 dust cases in the form of extra layers coated on fewer and larger dust particles. This effect has  
 264 been discussed in several previous studies [28,34]. This effect can also help explain the AOD  
 265 differences between the three coating schemes. As shown in Figure 3c the  $G_{total}$  of the coating  
 266 scheme 1 is the largest one among the three schemes, followed by scheme 2. The scheme 3 has  
 267 the smallest  $G_{total}$ . This is because given the same amount of sulfate, coating on smaller dust  
 268 particles (i.e., scheme 1) is more efficient in terms of increasing the surface area than coating on  
 269 larger dust particles (i.e., scheme 3). Therefore, we can conclude that the AOD differences at  
 270  $0.55 \mu\text{m}$  between the external mixing and coated dust cases, as well as the differences among  
 271 the three coated cases, are mainly caused by the differences in total cross sectional area of the  
 272 particles. Figure 3d shows the  $\langle \omega \rangle$  comparison. Evidently, the external mixture is less  
 273 absorptive than the coated dust cases. Among the three coating schemes, scheme 1 is more  
 274 scattering than the other schemes. This is probably because in scheme 1 coating is proportional  
 275 to dust size which means smaller dust particles have proportionally thicker coating making coated  
 276 particles behave more like sulfate in terms of  $\langle \omega \rangle$ . In contrast, in scheme 3 the coating is  
 277 proportional to dust volume, meaning that larger dust particles have more coated sulfate.

278 However, in terms of scattering vs. absorption, the dust component of the coated particle is still  
 279 dominant leading to a  $\langle \omega \rangle$  very close to that of pure dust.

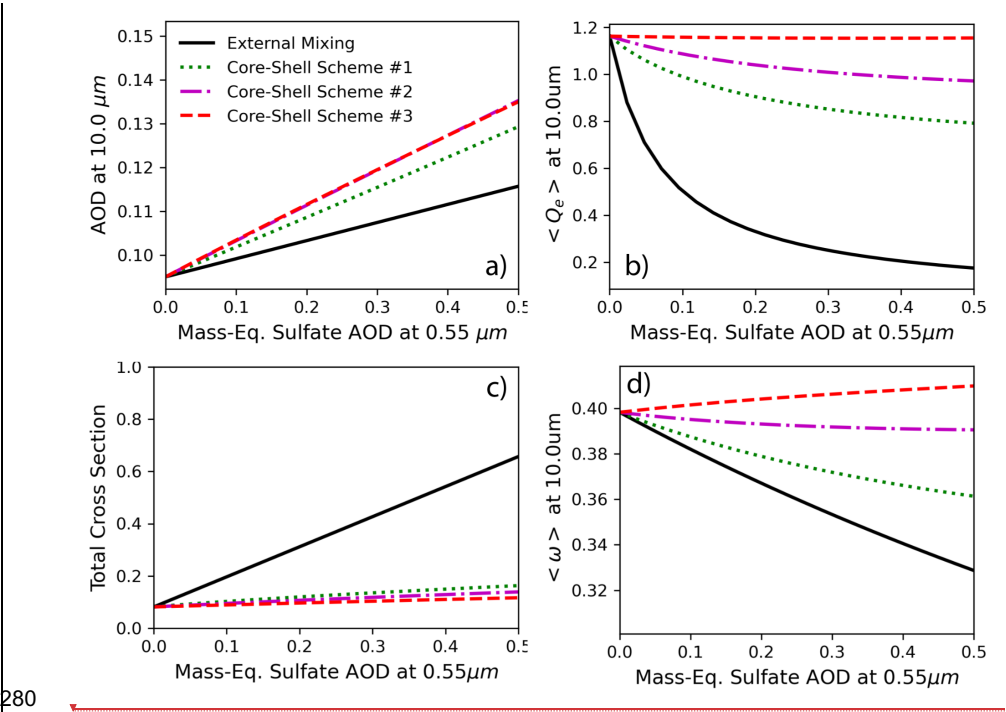
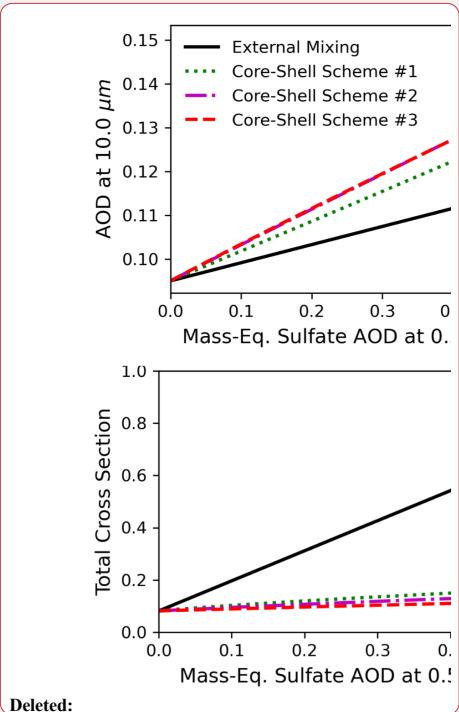


**Figure 4** Same as Figure 3 except for 10 $\mu$ m.

283 Turning to the results at 10  $\mu$ m in Figure 4, an important difference immediately emerges, that is  
 284 the AOD of external mixing is systematically smaller than those of coated dust cases (Figure 4a),  
 285 which is the opposite of the results for 0.55  $\mu$ m in Figure 3a. Because the geometrical cross  
 286 section (Figure 4c) is independent of the incident wavelength, this change of the order of AOD  
 287 must be a result of extinction efficiency  $\langle Q_e \rangle$ . As aforementioned in Table 2, the  $\langle Q_e \rangle$  of pure  
 288 sulfate is an order of magnitude smaller than that of dust at 10  $\mu$ m. In comparison, as shown in  
 289 Figure 4b, the  $\langle Q_e \rangle$  of coated dust cases are only slightly smaller to that of pure dust. Thus,



the the difference in  $\langle Q_e \rangle$  is the dominant factor at 10  $\mu\text{m}$ . Because of the small  $\langle Q_e \rangle$  of sulfate, the AOD of the external mixture increases much slower than that of coated dusts even though its geometrical cross section increases faster. Focusing on the three coated dust schemes, one can see the compromising effect of  $\langle Q_e \rangle$  and  $G_{total}$  on AOD. For example, the  $\langle Q_e \rangle$  of scheme #3 is larger than scheme #2 (Figure 4b) while the opposite is true for the  $G_{total}$  (Figure 4c). As a result their AODs as the products of  $\langle Q_e \rangle$  and  $G_{total}$  are almost identical. In Figure 4d, the  $\langle \omega \rangle$  of external mixture decreases as expected with sulfate AOD because the  $\langle \omega \rangle$  of sulfate is much smaller than that of dust due at 10  $\mu\text{m}$  to its small size (Table 2). Interestingly, the  $\langle \omega \rangle$  of the coated dust based on scheme #3 increases as more sulfate is added, i.e., thicker coating, although the change is very small.

If the external mixing is used as a reference, the results in Figure 4 and 5 reveal a contrasting impact of surface coating on the shortwave versus longwave scattering properties of dust particles. At 0.55  $\mu\text{m}$ , surface coating is much less effective in terms of AOD growth compared to external mixing mainly due to the effect of  $G_{total}$ . In contrast, at 10  $\mu\text{m}$ , surface coating is a more effective way to increase AOD due to the effect of  $\langle Q_e \rangle$ .

#### 4. Impacts of coating on dust DRE in SW and LW

In the last section, we compared the bulk scattering properties of the external mixing with those of coated dust cases at two typical SW and LW wavelengths. In this section, we extend the comparison to the whole SW and LW spectral region to investigate the impacts of dust-coating on the SW and LW aerosol DRE effects. The DRE of aerosol at the TOA and surface is defined as

$$DRE_{X,W} = F_{aer,X,W}^{\downarrow} - F_{clean,X,W}^{\downarrow},$$

Formatted: Outline numbered + Level: 1 + Numbering Style: 1, 2, 3, ... + Start at: 1 + Alignment: Right + Aligned at: 0.25" + Indent at: 0.5"

Formatted Table



315 In this definition, the subscript  $X$  indicates where the DRE is measured, i.e., TOA or surface,  
 316 subscript  $W$  indicates the spectral region of the DRE, i.e., SW or LW.  $F_{aer,X,W}^{\downarrow}$  is the net downward  
 317 broadband flux with aerosols and  $F_{clean,X,W}^{\downarrow}$  is the corresponding net downward broadband flux if  
 318 the aerosol is removed from the atmosphere and other things (e.g., atmosphere profiles and  
 319 surface properties) are kept the same. For an aerosol layer over dark ocean, the  $DRE_{TOA,SW}$  is  
 320 negative in general because aerosol reflection decreases the SW downward flux at TOA. In the  
 321 LW, the  $DRE_{TOA,LW}$  is generally positive as the absorption of aerosol in the LW reduces the  
 322 outgoing longwave radiation (OLR) contributed mostly by the warm ocean surface. Note that  
 323  $DRE_{TOA,SW}$  could switch to positive if the surface is highly reflective in which case aerosol  
 324 absorption of the surface reflection makes  $F_{aer,TOA,SW}^{\downarrow}$  larger than  $F_{clean,TOA,SW}^{\downarrow}$ . Similarly, in case  
 325 of a strong temperature inversion where aerosol layer temperature is warmer than the surface,  
 326 the  $DRE_{TOA,SW}$  could become negative because of stronger thermal emission by the aerosol layer  
 327 in comparison to the surface. The  $DRE_{Surf,SW}$  is generally negative because aerosol extinction  
 328 reduces the downward SW flux at surface in comparison with the clean condition if the aerosol is  
 329 removed, whereas the  $DRE_{Surf,LW}$  is generally positive as a result of the extra LW flux at the  
 330 surface emitted from the aerosol layer. On the basis of energy conservation, the DRE within the  
 331 atmosphere is defined as the difference between DRE at the TOA and surface, i.e.,  
 332

$$DRE_{Atmos,W} = DRE_{TOA,W} - DRE_{Surf,W}, \quad (3)$$

333 As such, a positive  $DRE_{Atmos,W}$  indicates that the atmosphere column absorbs more radiation due  
 334 to the presence of the aerosol layer, whereas a negative  $DRE_{Atmos,W}$  means that the aerosol layer  
 335 makes the atmosphere column absorb less radiation in comparison with the clean condition.  
 336

Formatted Table

The rapid radiative transfer model (RRTM) [35] is used to compute both SW and LW radiative fluxes for both aerosol-loaded ( $F_{aer,X,W}^{\downarrow}$ ) and aerosol-free ( $F_{clean,X,W}^{\downarrow}$ ) conditions. The RRTM retains reasonable accuracy in comparison with line-by-line results for single column calculations [35]. It divides the solar spectrum into 14 continuous bands ranging from 0.2 to 12.2  $\mu\text{m}$  and the thermal infrared (3.08–1000  $\mu\text{m}$ ) into 16 bands. Following the same procedures described in Section 3, we first computed the bulk scattering properties of coated dust based on three coating schemes, as well as the external mixing case for reference, for the 14 SW and 16 LW spectral bands of RRTM.

We took atmospheric profile and surface properties in April, 2007 over the region with latitude from 37N to 39N and longitude from 130E to 135E as an example to calculate the *diurnally averaged* dust DRE using RRTM following our previous studies [5,30]. The atmospheric profile, such as water vapor ( $\text{H}_2\text{O}$ ), ozone ( $\text{O}_3$ ) and temperature vertical profiles are from 3-hourly MERRA2 assimilated meteorological fields data [36]. Surface albedo in visible spectrum and surface emissivity are from MERRA2 1-hourly radiation diagnostics data. The 1-hourly data is averaged for every 3 hours to be consistent with the 3-hourly atmospheric profile data. We did not account for the spectral variation of surface properties, but considered their diurnal variations.

In the dust DRE calculations, we assume a 5-km geometric thickness of a well-mixed dust and sulfate mixture layer, ranging from 2 km up to 7 km. The temperature of the dust layer is 269 K at the bottom and 238 K at the top.

Formatted: Font: Times New Roman, 12 pt

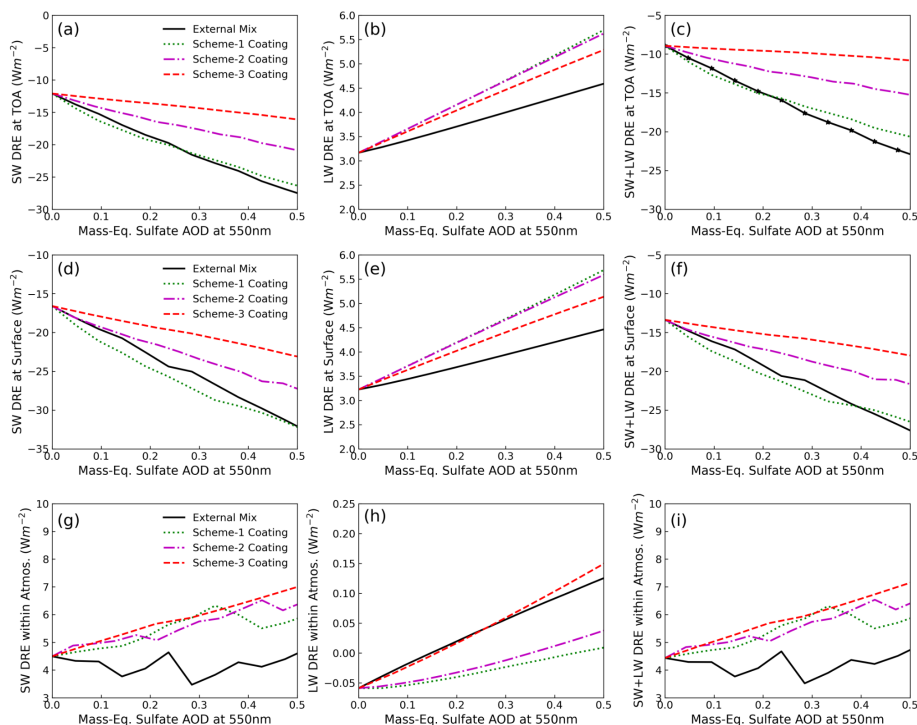
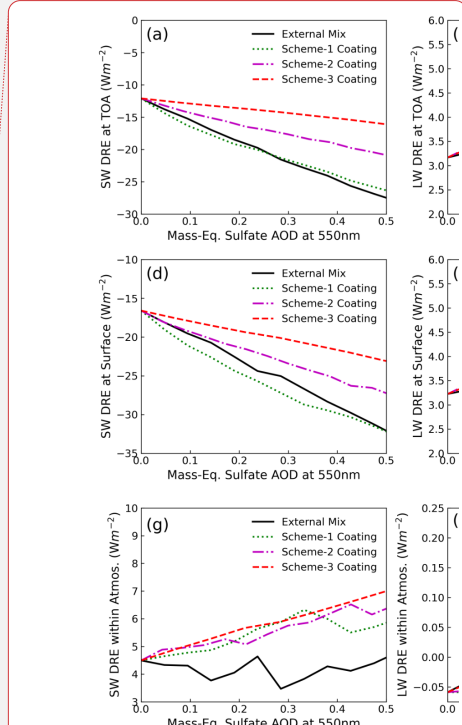


**Figure 5:** SW (left column), LW (middle column), and net DRE (right column) at TOA (top row), surface (middle row) and within the atmosphere (bottom row) for dust and sulfate mixtures. Solid line is for dust and sulfate external mixture, three dashed lines are for core-shell mixtures with three different schemes as shown in Table 2.

The DRE results from the RRTM are shown in Figure 5. At the TOA (top row of Figure 5), the external mixing and three coated dust cases all have a negative SW DRE (Figure 5a) and positive LW DRE (Figure 5c). But the order of their magnitudes is interesting. In the SW, the magnitude of the negative DRE of the external mixing increases quickly with the increasing sulfate AOD. Among the three coated dust schemes, the DRE of the scheme #1 increases the fastest, almost comparable with the external mixing. The scheme #3 is the slowest one. This is consistent with the slopes of  $0.55 \mu\text{m}$  AOD growth in Figure 3a and therefore probably shares the same

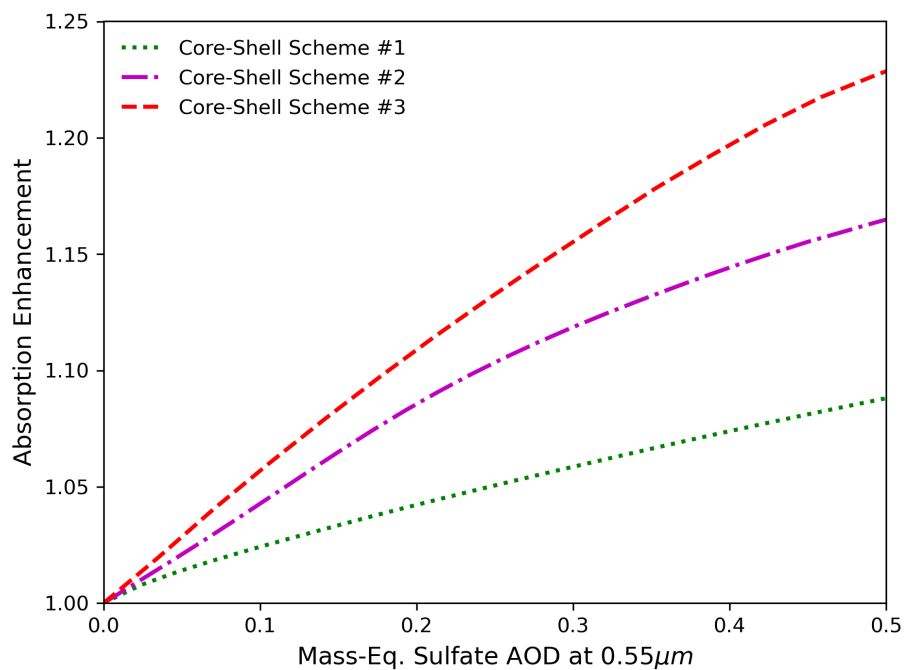


Deleted:

underlying physics. In the LW, the three coated dust cases have a significantly larger DRE (more positive) and also grow faster than the external mixing case, which is consistent with the 10  $\mu\text{m}$  AOD results in Figure 4b. What is most interesting and significant is that when SW and LW DREs are combined, the magnitude of the total DRE of the external mixing increases more than a factor of two from  $-8.9 \text{ W m}^{-2}$  for pure dust (sulfate AOD =0) to  $-22.9 \text{ W m}^{-2}$  for the mixture of dust AOD=0.2 and sulfate AOD=0.5 at 0.5  $\mu\text{m}$ . In contrast, the magnitude of the coated dust in scheme #1 increases only about 20% from  $-8.9 \text{ W m}^{-2}$  to  $-10.8 \text{ W m}^{-2}$ . From a different perspective, this implies that the total DRE at TOA by an externally mixed dust-sulfate layer is stronger (more negative), by more than a factor of two, than that of a layer where the same amount of sulfate is coated on the surface of dust particles (assuming scheme #3). This result also applied to the coated dust in scheme #2 although to a lesser extent. On the other hand, the coated dust in scheme #1 has the similar total DRE as the external mixing. The DRE results at the surface (middle row of Figure 5) are mostly consistent with those at the TOA.

The DRE within the atmosphere (bottom row of Figure 5) is obviously dominated by the SW component (Figure 5g) as the LW component is orders of magnitude smaller (Figure 5h). In comparison with the coated dust cases, the  $DRE_{Atmos,SW}$  of the external mixing is mostly independent of added sulfate. This is expected because sulfate is almost not absorptive in the SW. Thus, the added sulfate in the external mixture does not increase the overall SW absorption of the layer as the dust and sulfate particles mostly interact with the radiation separately and independently when multiple scattering is weak for small AOD. In contrast, there is a clear and significant increasing trend of  $DRE_{Atmos,SW}$  with added sulfate for the coated dust cases (Figure 5g). In other words, the coated sulfate layer, although non-absorptive itself in the SW, can increase the overall absorption of the dust in comparison with the pure dust. For example, the  $DRE_{Atmos,SW}$  for an external mixture of dust AOD=0.2 and sulfate AOD=0.5 (at 0.5  $\mu\text{m}$ ) is 4.5

398  $W m^{-2}$  in comparison with  $7.0 W m^{-2}$  if the same amount of sulfate is coated on the surface of  
 399 dust assuming scheme #3.  
 400



401  
 402 **Figure 6** Absorption Enhancement ratio due to coating.  
 403  
 404 The extra absorption of an absorbing core particle enhanced by the surface coated non-  
 405 absorptive material is known as the “lensing effect”. It was first discovered by Jacobson [37] and  
 406 studied extensively in the context of black carbon absorption enhancement due to the internal  
 407 mixing with other materials [38–42]. A commonly used parameter to quantify the the lensing effect  
 408 is the so-called absorption enhancement factor  $E_{Abs}$  which is defined as the ratio of the absorption  
 409 AOD (AAOD) of the coated particle to the AAOD of the core-particle without the coating. In the

context of this study, the  $E_{Abs}$  can be defined as the AAOD ratio between the coated dust and dust core. The variations of  $E_{Abs}$  for the three coated dust cases as a function of the sulfate AOD at 0.55  $\mu\text{m}$  are shown in Figure 6. Given the same amount of sulfate coating material, the lensing effect enhancement is most significant based on coating scheme #3, followed by scheme #2 and then #1. This is loosely consistent with the  $DRE_{Atmos,SW}$  results in Figure 5g. In comparison with the lensing effect on black carbon, the impacts of surface coating on dust absorption is far less studied. Nevertheless, because the focus of this study is on the contrasting impacts of surface coating on SW versus LW DRE of dust, a more in-depth study of the lensing effect on SW dust absorption will be left for future study.

## 5. Summary and Discussion

The mixing of transported dust and local pollution, e.g., sulfate, can result in coating of pollutants on the surface of the dust core, which in turn can modify the microphysical and radiative effects of dust. Many previous studies investigated the effects of surface coating on the scattering properties of dust particles in the solar SW spectral region and the consequential impacts on  $DRE_{SW}$ . In comparison, the corresponding impacts on the LW dust scattering properties and  $DRE_{LW}$  and the underlying physics are much less studied. This study fills this important gap in our understanding. Assuming the concentric spherical core-shell model for the coated dust, we developed three surface coating schemes to simulate potentially different coating mechanisms. The impacts of sulfate surface coating on the scattering properties of dust, as well as the DRE, in both SW and LW spectral regions were investigated through inter-comparisons between the three coating schemes and comparison with the external mixing scenario. The key findings are:

1. At 0.55  $\mu\text{m}$ , the AOD of sulfate-dust external mixing has the highest AOD increasing efficiency with increasing sulfate. The AOD of scheme #1 increases faster than the other two schemes. At 10  $\mu\text{m}$ , the order of AOD increasing rates is reversed, with the coated

Formatted: Outline numbered + Level: 1 + Numbering  
Style: 1, 2, 3, ... + Start at: 1 + Alignment: Right + Aligned  
at: 0.25" + Indent at: 0.5"

Formatted: Outline numbered + Level: 1 + Numbering  
Style: 1, 2, 3, ... + Start at: 1 + Alignment: Left + Aligned  
at: 0.25" + Indent at: 0.5"

dust cases increasing faster than the external mixing. A further analysis reveals that the dominant factor for the AOD growth is different in SW from that in LW. The increasing rate of  $G_{total}$  (total geometrical cross section) is the dominant reason that explains why external mixing has a higher AOD growth rate in comparison with coated dust cases in the SW. In contrast, the increasing rate of  $\langle Q_e \rangle$  (extinction efficiency) is the dominant factor in the LW.

2. The order of  $DRE_{TOA}$  and  $DRE_{surf}$  loosely follows the order of AOD, i.e., the external mixing has the strongest negative cooling  $DRE_{TOA,SW}$  ( $DRE_{surf,SW}$ ) and the weakest warming  $DRE_{TOA,LW}$  ( $DRE_{surf,LW}$ ) in comparison with the coated dust cases.
3. The SW absorption of coated dust cases is significantly enhanced by the lensing effect of coated sulfate resulting in significantly more positive  $DRE_{Atmos,SW}$  in comparison with that of both external mixing and pure dust core.

To our best knowledge, this study is the first to reveal that the AOD growth of the pollution-dust mixture is dominated by different factors in the LW than in the SW. While our study is theoretical in nature, it paved the way for future investigations of the impacts of surface coating on the DRE of dust on climate based on, for example, satellite observations (see Figure 1) and model simulations. In particular, our study suggests that simply treating the pollution-dust mixture as external mixing, when a considerable fraction is internally mixed (i.e., coated dust), can lead to a significant overestimate of the cooling effect of dust in the SW and underestimation of the warming effect of dust LW. When SW and LW summed together, the total DRE of external mixing is substantially more negative than the coated dust. Furthermore, our study also reveals that the lensing effect of surface coating can significantly enhance the absorption of dust, which can not be properly simulated by either pure dust or external mixing of dust and pollution. These interesting and important effects of surface coating on dust particles will be further investigated in future observation based studies.

460 **Declaration of competing interest**

461 The authors declare that they have no known competing financial interests or personal  
462 relationships that could have appeared to influence the work reported in this paper.

463

464 **Acknowledgments**

465 Z. Zhang acknowledges funding support from NSF (AGS-2232138). H. Yu was supported by  
466 NASA CloudSat/CALIPSO program and MEASURES program. The computations in this study  
467 were performed at the UMBC High Performance Computing Facility (HPCF). The facility is  
468 supported by the US National Science Foundation through the MRI program (grant nos. CNS-  
469 0821258 and CNS-1228778) and the SCREMS program (grant no. DMS-0821311), with  
470 substantial support from UMBC.



471

472 **References:**

473

- 474 [1] Boucher O, Randall D, Artaxo P, Bretherton C, Feingold G, Forster P, et al. Clouds and  
475 aerosols, Cambridge, United Kingdom and New York, NY, USA: Cambridge University Press;  
476 2013, p. 571–657. <https://doi.org/10.1017/cbo9781107415324.016>.
- 477 [2] Textor C, Schulz M, Guibert S, Kinne S, Balkanski Y, Bauer S, et al. Analysis and  
478 quantification of the diversities of aerosol life cycles within AeroCom. *Atmos Chem Phys*  
479 2006;6:1777–813. <https://doi.org/10.5194/acp-6-1777-2006>.
- 480 [3] Yu H, Kaufman YJ, Chin M, Feingold G, Remer LA, Anderson TL, et al. A review of  
481 measurement-based assessments of the aerosol direct radiative effect and forcing. *Atmos*  
482 *Chem Phys* 2006;6:613–66. <https://doi.org/10.5194/acp-6-613-2006>.
- 483 [4] Kok JF, Ridley DA, Zhou Q, Miller RL, Zhao C, Heald CL, et al. Smaller desert dust cooling  
484 effect estimated from analysis of dust size and abundance. *Nat Geosci* 2017;10:274–8.  
485 <https://doi.org/10.1038/ngeo2912>.
- 486 [5] Song Q, Zhang Z, Yu H, Kato S, Yang P, Colarco P, et al. Net radiative effects of dust in the  
487 tropical North Atlantic based on integrated satellite observations and in situ measurements.  
488 *Atmos Chem Phys* 2018;18:11303–22. <https://doi.org/10.5194/acp-18-11303-2018>.
- 489 [6] Song Q, Zhang Z, Yu H, Kok JF, Biagio CD, Albani S, et al. Size-resolved dust direct  
490 radiative effect efficiency derived from satellite observations. *Atmos Chem Phys*  
491 2022;22:13115–35. <https://doi.org/10.5194/acp-22-13115-2022>.
- 492 [7] Helmert J, Heinold B, Tegen I, Hellmuth O, Wendisch M. On the direct and semidirect effects  
493 of Saharan dust over Europe: A modeling study. *J Geophys Res Atmospheres* 2007;112.  
494 <https://doi.org/10.1029/2006jd007444>.
- 495 [8] Huang J, Lin B, Minnis P, Wang T, Wang X, Hu Y, et al. Satellite-based assessment of  
496 possible dust aerosols semi-direct effect on cloud water path over East Asia. *Geophys Res Lett*  
497 2006;33. <https://doi.org/10.1029/2006gl026561>.
- 498 [9] Karydis VA, Kumar P, Barahona D, Sokolik IN, Nenes A. On the effect of dust particles on  
499 global cloud condensation nuclei and cloud droplet number. *J Geophys Res Atmospheres* 1984  
500 2012 2011;116:n/a-n/a. <https://doi.org/10.1029/2011jd016283>.
- 501 [10] Hoose C, Möhler O. Heterogeneous ice nucleation on atmospheric aerosols: a review of  
502 results from laboratory experiments. *Atmos Chem Phys* 2012;12:9817–54.  
503 <https://doi.org/10.5194/acp-12-9817-2012>.
- 504 [11] Prospero JM. The Impact of Desert Dust Across the Mediterranean. *Envir Sci Tech Lib*  
505 1996;133–51. [https://doi.org/10.1007/978-94-017-3354-0\\_13](https://doi.org/10.1007/978-94-017-3354-0_13).
- 506 [12] Engelstaedter S, Tegen I, Washington R. North African dust emissions and transport.  
507 *Earth-Sci Rev* 2006;79:73–100. <https://doi.org/10.1016/j.earscirev.2006.06.004>.
- 508 [13] Guo J, Lou M, Miao Y, Wang Y, Zeng Z, Liu H, et al. Trans-Pacific transport of dust  
509 aerosols from East Asia: Insights gained from multiple observations and modeling. *Environ*  
510 *Pollut* 2017;230:1030–9. <https://doi.org/10.1016/j.envpol.2017.07.062>.
- 511 [14] Hanisch F, Crowley JN. The heterogeneous reactivity of gaseous nitric acid on authentic  
512 mineral dust samples, and on individual mineral and clay mineral components. *Physical*  
513 *Chemistry Chemical Physics* 2001;3:2474–82. <https://doi.org/10.1039/b101700o>.

514 [15] Jordan CE, Dibb JE, Anderson BE, Fuelberg HE. Uptake of nitrate and sulfate on dust  
515 aerosols during TRACE-P. *J Geophys Res Atmospheres* 1984 2012 2003;108.  
516 <https://doi.org/10.1029/2002jd003101>.

517 [16] Sullivan RC, Guazzotti SA, Sodeman DA, Prather KA. Direct observations of the  
518 atmospheric processing of Asian mineral dust. *Atmospheric Chemistry and Physics*  
519 2007;7:1213–36. <https://doi.org/10.5194/acp-7-1213-2007>.

520 [17] Li WJ, Shao LY. Observation of nitrate coatings on atmospheric mineral dust particles.  
521 *Atmos Chem Phys* 2009;9:1863–71. <https://doi.org/10.5194/acp-9-1863-2009>.

522 [18] Hand VL, Capes G, Vaughan DJ, Formenti P, Haywood JM, Coe H. Evidence of internal  
523 mixing of African dust and biomass burning particles by individual particle analysis using  
524 electron beam techniques. *J Geophys Res Atmospheres* 1984 2012 2010;115.  
525 <https://doi.org/10.1029/2009jd012938>.

526 [19] Pan X, Uno I, Wang Z, Nishizawa T, Sugimoto N, Yamamoto S, et al. Real-time  
527 observational evidence of changing Asian dust morphology with the mixing of heavy  
528 anthropogenic pollution. *Sci Rep-Uk* 2017;7:335. <https://doi.org/10.1038/s41598-017-00444-w>.

529 [20] Winker DM, Tackett JL, Getzewich BJ, Liu Z, Vaughan MA, Rogers RR. The global 3-D  
530 distribution of tropospheric aerosols as characterized by CALIOP. *Atmos Chem Phys*  
531 2013;13:3345–61. <https://doi.org/10.5194/acp-13-3345-2013>.

532 [21] Underwood GM, Song CH, Phadnis M, Carmichael GR, Grassian VH. Heterogeneous  
533 reactions of NO<sub>2</sub> and HNO<sub>3</sub> on oxides and mineral dust: A combined laboratory and modeling  
534 study. *J Geophys Res Atmospheres* 2001;106:18055–66. <https://doi.org/10.1029/2000jd900552>.

535 [22] Ullerstam M, Vogt R, Langer S, Ljungström E. The kinetics and mechanism of SO<sub>2</sub>  
536 oxidation by O<sub>3</sub> on mineral dust. *Phys Chem Chem Phys* 2002;4:4694–9.  
537 <https://doi.org/10.1039/b203529b>.

538 [23] Usher CR, Michel AE, Grassian VH. Reactions on Mineral Dust. *Chem Rev*  
539 2003;103:4883–940. <https://doi.org/10.1021/cr020657y>.

540 [24] Tian P, Zhang L, Ma J, Tang K, Xu L, Wang Y, et al. Radiative absorption enhancement of  
541 dust mixed with anthropogenic pollution over East Asia. *Atmos Chem Phys* 2018;18:7815–25.  
542 <https://doi.org/10.5194/acp-18-7815-2018>.

543 [25] Riemer N, Ault AP, West M, Craig RL, Curtis JH. Aerosol Mixing State: Measurements,  
544 Modeling, and Impacts. *Rev Geophys* 2019;39:4767. <https://doi.org/10.1029/2018rg000615>.

545 [26] Cziczo DJ, Froyd KD, Gallavardin SJ, Moehler O, Benz S, Saathoff H, et al. Deactivation of  
546 ice nuclei due to atmospherically relevant surface coatings. *Environ Res Lett* 2009;4:044013.  
547 <https://doi.org/10.1088/1748-9326/4/4/044013>.

548 [27] Tian Y, Pan X, Wang Z, Wang D, Ge B, Liu X, et al. Transport Patterns, Size Distributions,  
549 and Depolarization Characteristics of Dust Particles in East Asia in Spring 2018. *J Geophys Res*  
550 *Atmospheres* 2020;125. <https://doi.org/10.1029/2019jd031752>.

551 [28] Bauer SE, Mishchenko MI, Lacis AA, Zhang S, Perlwitz J, Metzger SM. Do sulfate and  
552 nitrate coatings on mineral dust have important effects on radiative properties and climate  
553 modeling? *J Geophys Res Atmospheres* 1984 2012 2007;112:D17202.  
554 <https://doi.org/10.1029/2005jd006977>.

555 [29] Biagio CD, Balkanski Y, Albani S, Boucher O, Formenti P. Direct Radiative Effect by  
556 Mineral Dust Aerosols Constrained by New Microphysical and Spectral Optical Data. *Geophys*  
557 *Res Lett* 2020;47. <https://doi.org/10.1029/2019gl086186>.

- [30] Song Q, Zhang Z, Yu H, Kok JF, Biagio CD, Albani S, et al. Size-Resolved Dust Direct Radiative Effect Efficiency Derived from Satellite Observations. *Atmospheric Chem Phys Discuss* 2022;2022:1–44. <https://doi.org/10.5194/acp-2022-350>.
- [31] Yu H, Chin M, Bian H, Yuan T, Prospero JM, Omar AH, et al. Quantification of trans-Atlantic dust transport from seven-year (2007–2013) record of CALIPSO lidar measurements. *Remote Sens Environ* 2015;159. <https://doi.org/10.1016/j.rse.2014.12.010>.
- [32] Song Q, Zhang Z, Yu H, Ginoux P, Shen J. Global dust optical depth climatology derived from CALIOP and MODIS aerosol retrievals on decadal timescales: regional and interannual variability. *Atmos Chem Phys* 2021;21:13369–95. <https://doi.org/10.5194/acp-21-13369-2021>.
- [33] Sumlin BJ, Heinsohn WR, Chakrabarty RK. Retrieving the aerosol complex refractive index using PyMieScatt: A Mie computational package with visualization capabilities. *J Quant Spectrosc Radiat Transf* 2018;205:127–34. <https://doi.org/10.1016/j.jqsrt.2017.10.012>.
- [34] Bauer SE, Koch D. Impact of heterogeneous sulfate formation at mineral dust surfaces on aerosol loads and radiative forcing in the Goddard Institute for Space Studies general circulation model. *J Geophys Res Atmospheres* 1984 2012 2005;110. <https://doi.org/10.1029/2005jd005870>.
- [35] Mlawer EJ, Taubman SJ, Brown PD, Iacono MJ, Clough SA. Radiative transfer for inhomogeneous atmospheres: RRTM, a validated correlated-k model for the longwave. *J Geophys Res Atmospheres* 1997;102:16663. <https://doi.org/10.1029/97jd00237>.
- [36] Gelaro R, McCarty W, Suarez MJ, Todling R, Molod A, Takacs L, et al. The Modern-Era Retrospective Analysis for Research and Applications, Version 2 (MERRA-2). *J Climate* 2017;30:5419–54. <https://doi.org/10.1175/jcli-d-16-0758.1>.
- [37] Jacobson MZ. Strong radiative heating due to the mixing state of black carbon in atmospheric aerosols. *Nature* 2001;1–3.
- [38] Zhang R, Khalizov AF, Pagels J, Zhang D, Xue H, McMurry PH. Variability in morphology, hygroscopicity, and optical properties of soot aerosols during atmospheric processing. *Proc National Acad Sci* 2008;105:10291–6. <https://doi.org/10.1073/pnas.0804860105>.
- [39] Zhang Y, Favez O, Canonaco F, Liu D, Močnik G, Amodeo T, et al. Evidence of major secondary organic aerosol contribution to lensing effect black carbon absorption enhancement. *Npj Clim Atmos Sci* 2018;1:47. <https://doi.org/10.1038/s41612-018-0056-2>.
- [40] Lack DA, Cappa CD. Impact of brown and clear carbon on light absorption enhancement, single scatter albedo and absorption wavelength dependence of black carbon. *Atmos Chem Phys* 2010;10:4207–20. <https://doi.org/10.5194/acp-10-4207-2010>.
- [41] Liu D, Whitehead J, Alfara MR, Reyes-Villegas E, Spracklen DV, Reddington CL, et al. Black-carbon absorption enhancement in the atmosphere determined by particle mixing state. *Nat Geosci* 2017;10:184–8. <https://doi.org/10.1038/ngeo2901>.
- [42] Bond TC, Habib G, BERGSTROM RW. Limitations in the enhancement of visible light absorption due to mixing state. *J Geophys Res Atmospheres* 1984 2012 2006;111:360. <https://doi.org/10.1029/2006jd007315>.